Journal of Petroleum Science and Technology 11(3): 31, 2021, Pages 2-10
DOI: 10.22078/JPST.2021.4540.1751

Journal of Petroleum Science and Technology

https://jpst.ripi.ir/

Evaluation of Rock Properties Determined from Core and NMR Data: A Case Study on Asmari Carbonate Reservoir

Mehdi Shabani*, Sima Ghaffary and Saeed Yarmohammadi
Department of Petroleum Engineering, Amirkabir University of Technology, Tehran, Iran

Abstract
A detailed description of the carbonate reservoir is an important step in preparing a field development plan. An accurate determination of petrophysical parameters and rock characteristics are key parameters in the carbonate reservoir description. The rock properties are traditionally obtained from different techniques such as lab measurement, well logging, well test, etc. In this manuscript, data from core measurements and NMR measurements are analyzed to study the petrophysical properties of Cretaceous carbonate rock from Asmari Formation. First, the pore size, pore system, porosity and permeability are determined from the core measurements and NMR Analysis. Second, the results of core and NMR evaluations are compared, and the reasons for differences are distinguished. Comparison between the porosity values demonstrates that porosity from NMR and helium injection experiments are very similar in which the average porosity is 21.4 % and NMR porosity is 20.68%. Afterwards, pore sizes received from the NMR model show reliable results and match the pore size distribution determined from the MICP experiment. The permeability value is modeled with NMR permeability predicting models, namely Standard Kenyon and Timur-Coates. Adjusted NMR Permeability results are 17.7 (mD) and 18 (mD) for (SDR) and (TC) methods, respectively, and they are consistent with laboratory core permeability results (Kg=22, Kl=19.2, Kw=18.4). The pore throat distributions are also similar for two NMR and core measurement methods. This study shows how NMR analysis could be useful in determining petrophysical parameters. Ultimately, the results for reservoir characteristics of carbonate rock obtained by core and NMR experiments are compared quantitatively and qualitatively.

Keywords: NMR, Core Measurement, Permeability, Porosity, Pore Size Distribution, SDR and Timur-Coates Models, Thin Section.

Introduction
Heterogeneity and complexity of Carbonate formations make the reservoir characterization studies and field development plan more difficult, in particular when comprehensive petrophysical data are not available [1]. To know reservoir quality and architecture, the petrophysical and geological properties of the reservoir should be investigated in an integrated study [2]. Among the petrophysical reservoir parameters, porosity and permeability, grain density, pore type and pore structure are considered key parameters for static reservoir modeling [3]. There are some conventional ways to study the rock properties of carbonate formations, including core measurements, well logging data, and well tests [4]. Using the new method of nuclear magnetic resonance (NMR) could be considered a potential technique for rock sample petrophysical studies [5]. The NMR method could also be utilized to confirm the petrophysical properties estimated from other methods. In many cases, a comparison of core and NMR is used for the basic rock properties validation [6].

Core catching provides some samples that are known as representative of reservoir formation. Core sample analysis in laboratories follows different objectives in terms of (1) geological, (2) petrophysical and (3) reservoir studies. In the geological study, lithological properties, sedimentary textures and structures, diagenesis processes, fossil content and other facies aspects could be investigated in macroscopic and microscopic scales [7]. From a petrophysical point of view, reservoir quality data (porosity and permeability), saturation parameters, grain density and rock physics properties could be received from the core laboratory [8]. Reservoir engineers also use core laboratory data to find dynamic reservoir information such as relative permeability, wettability and capillary pressure data [9]. The abovementioned data are calculated in conventional core measurement (CCAL) and special core experiments (SCAL).

Notably, the experiments condition and data processing methods are important to gain valid and reliable laboratory data [10].

*Corresponding author: Mehdi Shaabani, *Department of Petroleum Engineering, Amirkabir University of Technology, Tehran, Iran*
E-mail addresses: mehdi.shabani@aut.ac.ir
Received 2021-07-03, Received in revised form 2021-11-17, Accepted 2021-11-22, Available online . 2022-05-15....

The NMR technique has rapidly developed within two past decades to be a practical tool for investigating the reservoir rock [11, 12, 13]. The results from the NMR technique are used to investigate pore systems, porosity and permeability, capillary pressure and fluid movement behavior data such as irreducible water saturation estimation and relative permeability determination. The NMR analysis is performed by using a low field NMR Spectrometer (2 MHz). The measured raw NMR signals are converted to a standard relaxation T_2 distribution [14]. The T_2 relaxation time spectrum is analyzed for the rock properties interpretation. Many researchers have used NMR data and core measurement to correlate and interpret various rock properties [12, 15, 16]. The MICP capillary pressure and NMR data have been used to determine irreducible water saturation and permeability. The T_2 distribution method has been used to investigate pore structure and the pore size distribution from capillary pressure [17]. The NMR and MICP data with percolation theory have been used to understand porous media better [18]. A wide pore size window was concluded with high percolation thresholds. A methodology for NMR data has been used to identify movable fluid distribution in tight sandstones. A formulation has been introduced to use the relativity of the surface to calculate the pore size from NMR data [13]. The NMR results have been compared with the pore sizes determined from images analysis. The T_2 values have been converted to the dynamic modeling parameters, Pc and Kr curves [2]. They have compared the results with the laboratory-derived MICP and Kr curves for developing rock typing in carbonate rock reservoirs.

In sandstone rock, the petrophysical properties are usually a function of porosity, while in carbonate rock, samples do not show a simple relationship with porosity [19]. It is because carbonates are heterogeneous with variation in pore distribution, pore connectivity and pore types. Problems and solutions have been addressed when using the NMR data for evaluating carbonate rock [20].

However, in the current study, data from core and NMR experiments are used to study petrophysical properties such as pore throat size, porosity, permeability, immobile and movable fluid in pore spaces. For the permeability estimation, two models of Standard Kenyon (SDR) and Timur-Coates (TC) are developed to simulate core permeability by NMR permeability predictors for the Asmari Formation in an Iranian oilfield. The Asmari Formation is composed of carbonate with a large sedimentary sequence identified in the Zagros Basin. The age of Asmari Formation is Oligocene to the lower Miocene [21]. The lower part is limestone, while the upper parts are dolostones. However, this formation is considered an important productive layer in most oilfields in the southwest of Iran. The lithology of the Asmari Formation in the candidate oilfield indicates a low vertical lithological variation.

Geological Platform

The Oligocene-Miocene aged Asmari Formation is one of the most oil-bearing reservoirs in Dezful Embayment. As seen in Figure 1, Dezful Embayment is a basin in the Zagros fold-thrust belt that covers an area of 60,000 sq. km in the Southwest of Iran [22]. Field structures in this area are elliptical anticlines formed due to the collision of the Persian and the Arabian Plates. The main lithology of the Asmari Formation includes limestone, dolomite, sandstone, anhydrite, siltstone and shale. Furthermore, Asmari formation is placed on the Pabdeh Formation (Paleocene- Oligocene), under unconformable contact of the Gachsaran Formation (Middle Miocene), as seen in Figure 2 [23]. Detailed geological and petrophysical analyses show that Asmari Formation is deposited in a distally steepened ramp platform. The maximum thickness of the Asmari Formation is in the northeastern corner of the Dezful Embayment [24].

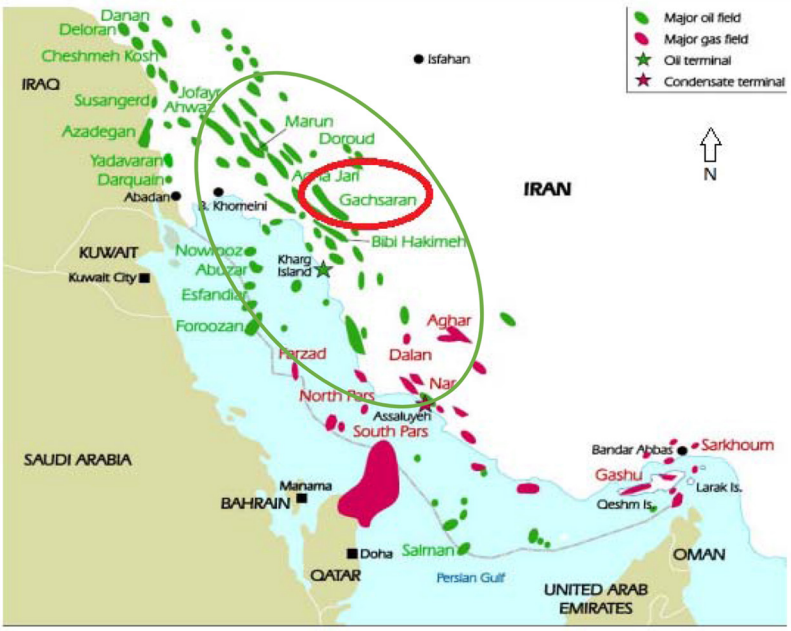

Fig.1 Location map of Dezful embayment oil fields in South-west of Iran

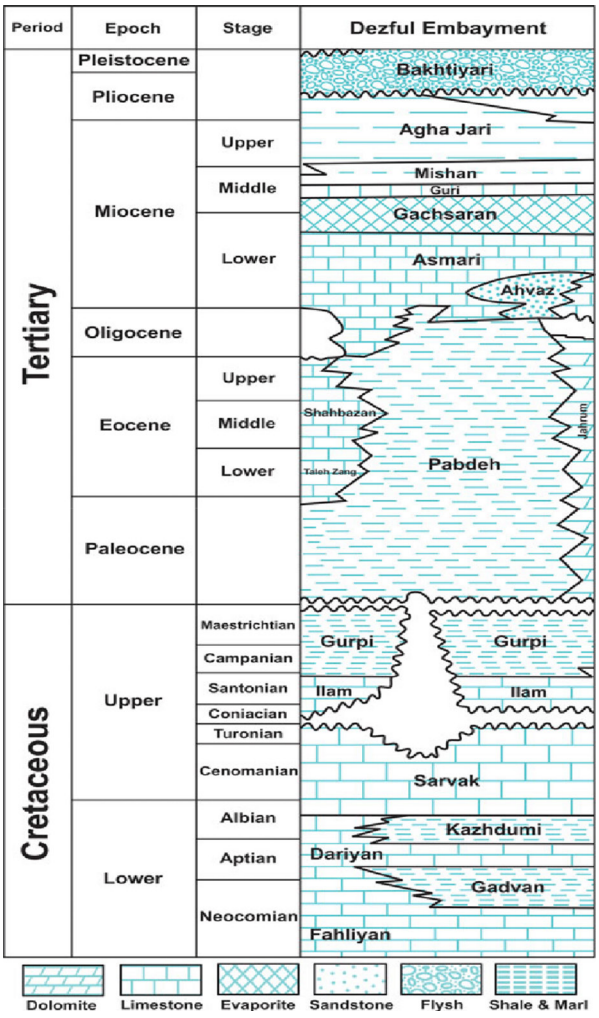

Fig. 2 Stratigraphic chart of Cretaceous-Tertiary Dezful Embayment illustrating the main source rocks, reservoirs and seals in the area [25].

Materials and Methods

Asmari Formation petrophysical and geological data received from core lab analysis and NMR technique are investigated in this study. The data contains basic core properties (pore size distribution, grain density, porosity, and permeability) and NMR analysis data from a carbonate rock sample. A thin section is also prepared by cutting off the studied core sample. The core plug measurements and thin-section images are carefully evaluated as real samples for confirmation of NMR results. Laboratory NMR measurement on the plug is also performed as the main goal of this study, and its results are compared with the core measurement. However, the detailed procedure is given as follows.

Core Measurements

The core plug is initially cleaned by using the Soxhlet cleaning technique in refluxing the Soxhlet extractor with a mixture of methanol and toluene. The main objective of this design is to enable efficient solvent cleaning of the core sample without damaging the pore system. The technique consists of a flask where the solvent (a mixture of Methanol and Toluene) is boiled. The vapor is directed into a condenser which is above the core sample chamber. The condensed solvent is falling down into the sample, and when the solvent reaches above the top of the highest core sample, it is run off back into the original solvent boiling flask. This process is repeated until the sample is cleaned. After the sample cleaning step, the sample is dried in an oven at 60 °C. When the weight remains constant, it is considered that the drying process is completed. The dry sample is then placed in a desiccator and cooled at room temperature. The desiccator is used to avoid moisture contamination on the sample from the atmosphere. The grain volume of the sample is accurately measured by using a helium gas Porosimeter. The porosimeter is calibrated before the measurement. The dry sample is weighted and then loaded into the special container, and the helium has flowed. With the measurement of pore volume and the bulk volume of the sample, the porosity and grain density are determined by the following equations:

$$porosity\ (\phi) = \frac{v_p}{v_b} \times 100 \quad (1)$$

$$graindensity\ = (\rho) = \frac{W_t}{V_g} \quad (2)$$

where, Vp, Vb and Vg are total volumes in cc for pores, bulk and grain, respectively, and wt is the dry sample weight in gram.

The absolute gas permeability of the dry sample is measured with a calibrated permeameter. The nitrogen is the flowing medium, and the flow is stabilized before the reading. The gas permeability is, however, determined by the following Darcy law:

$$K_g = \frac{Q}{A} \frac{\mu P_A L\, 2000}{\left[(P_2 + P_A)^2 - (P_z + P_A)^2\right]} \quad (3)$$

where, L (length, cm), D (diameter, cm), and A (cross-section area, cm^2) represents the sample dimension, μ is gas viscosity (centipoise), and Q is the gas flow rate (cc/s). P_A, P_1 and P_2 are pressure of atmospheric, inlet pressure, and outlet pressure, respectively.

Primary drainage capillary pressure is determined by injecting mercury into the sample. A small cut-off from the clean core sample is used. The sample is first weighed and then placed into the penetrometer for mercury injection. The pressure is increased at a stepwise program up to 60000 psi, and the volume of injected mercury is read. However, the distribution of pores is calculated by the capillary pressure data and the Young Laplace Equation as follows:

$$P_C = \frac{2\delta \cos(\theta)}{r} \quad (4)$$

where, Pc is capillary pressure (dynes/cm^2), δ is the surface tension of mercury (485 dynes/cm^2), ϕ is contact angle, mercury/solid (130°), and r is pore entry radius (cm).

A thin section slice has been prepared from the cut-off taken from the core sample. The thin section is colored with alizarin Red-S and blue dye resin. The thin section image is analyzed to reveal the pore structure of the core sample. The result is usually used to interpret the basic rock properties and rock characterization concerning sedimentary fabric and texture, cementation, grain and clay mineralogy, and reservoir quality [26, 3].

NMR measurement is performed by using a low field NMR Spectrometer (2 MHz). The true T_2 of the sample has been measured by CPMG (Carr-Purcell-Meiboom-Gill) sequence

with a 90 magnetic pulse. The CPMG sequence removes dephasing effects due to possible magnet inhomogeneities, and the pulse sequence also eliminates the effects of variations of the magnetic field. However, the T_2 relaxation time spectrum is determined by fitting the CPMG curve to the following equation.

$$M = \sum_i M_o^i \exp\left(-\frac{t}{T_z^i}\right) \quad (5)$$

where, M is the initial magnetization at time zero and T_2^i is constant for the T_2 relaxation time

Pore Size Distribution

When a fluid is placed into a pore system, the interaction of the fluid with the pore surfaces will cause a quickening of the T_2 relaxation time compared to the relaxation time of bulk fluid T_{2bulk}. In smaller pores, there is a greater surface-to-volume ratio so that the fluid frequently interacts with the pore walls, and it will lead to shorter relaxation times. In larger pores, there is a larger surface-to-volume ratio; thus, the fluid interacts less with the pore walls, resulting in longer relaxation times [27]. The following equation expresses the relationship for this behavior:

$$\frac{1}{T_z} = \rho_2 \frac{S}{V} \quad (6)$$

where T_2 is measured relaxation time (ms), ρ_2 is surface relaxation constant, S is pore surface area (cm^2), and V is pore volume (cm^3)

In Equation 6, the ratio of pore surface to pore volume (S/V) is determined by

$$\frac{S}{V} = \frac{F_S}{r} \quad (7)$$

where r is the radius of the pore throat; F_S is the shape factor related to the pore throat. The F_S value is 2 for the cylindrical pore and 3 for the spherical pore. By considering Equations (6) and (7), it is possible to relate NMR T_2, and pore throat size (r) and the relationship is given in the following:

$$T_2 = \frac{r}{\rho_S F_S} \quad (8)$$

As a general for, the relationship between the pore size and T_2 distribution is linear and presented as follows:

$$r = C \times T_2 \quad (9)$$

where C ($C = \rho_s . F_S .$) is the constant value for conversion. It is usually obtained by linear regression with respect to the pore size determined from NMR measurement [17, 28].

For the porous medium, the pore system is assumed to be a number of interconnected pores rather than closed pores. Therefore, all pores have their T2 value and signal amplitude. The sample is fully saturated with one fluid (e.g., salt formation water); therefore, the T2 data which are obtained from the saturated sample is an indicator of the distribution of pores in the rock sample [29, 30, 31, 32].

Porosity

A reference fluid with 20 ml of 50,000 ppm NaCl has been used, and it is placed in a vial with enough sealed to prevent evaporation. A standard T_2 measurement has been made upon the fluid sample. This value is used to convert the NMR signal into fluid volume. The core plug is saturated with a similar fluid, and CPMG measurement is then performed on the core plug sample. NMR porosity is determined by the following equation [33, 34].

$$\phi = \frac{M}{M_O} \times \frac{V_O}{V} \times 100 \quad (10)$$

where ϕ is porosity (percent), M is total amplitude in saturated core sample, Mo is total amplitude in reference fluid, Vo is fluid reference volume (cc), and V is the bulk volume of the core sample (cc).

Permeability

Kenyon Schlumberger-Doll-Research (SDR) and Timur-Coates (TC) techniques are two well-known methods used for calculating NMR permeability [35, 36, 37, 38]. Although the two methods are similar in form, the Kenyon method has an advantage over the TC method. It only needs to be performed on 100% water-saturated plug samples, while the TC method requires the NMR measurement upon both 100% saturated and desaturated plug samples. The latter can also be used in systems containing both oil and water [12]. Both methods are friendly and fast to produce reliable data. The methods need other data from NMR measurements (porosity and pore size) to determine the permeability. However, a detailed description for each permeability model is given in the following:

a. Kenyon (SDR) Permeability

The T_0 distribution data is used to estimate permeability by using the Kenyon (or SDR) equation [36]. This method relates the average T_2 time and plug sample porosity to permeability using the standard Kenyon (SDR) equation of the following form:

$$K\,(mD) = C\left[(T_{2LM})^a \left(\frac{\phi}{10}\right)^b\right] \quad (11)$$

where: T_{2LM} is mean T_2 value (logarithm), ϕ is porosity determined from NMR (percent), C is constant value to convert NMR permeability unit, and a and b are variable parameters.

The standard SDR equation sets the values of a=2, b=4 and c=1 x 10^{-3}. These values are usually optimized using a basic non-negative least squares calculation. However, these values are only average values, and in many situations, the variables are adjusted to match the resultant Kenyon permeability with measured brine permeability.

Timur-Coates (TC) Permeability

When NMR measurements are performed on the saturated and desaturated core sample, permeability can be calculated by using the Timur-Coates (TC) method. The method is related to the volumes of movable and immobile fluid and the porosity of the plug sample.The standard Timur-Coates equation (Equation 12) given as follows used to predict the permeability.

$$K\,(mD) = C\left[\left(\frac{FFI}{BVI}\right)^a \left(\frac{\phi}{10}\right)^b\right] \quad (12)$$

where FFI and BVI represent the index of movable fluid and immobile fluid, respectively, ϕ is porosity (percent), C is constant value to convert NMR permeability unit, and *a* and *b* are variable parameters.

The standard Timur-Coates equation sets the values of a=2, b=4 and c=1 x 10^{-3}. These values are optimized using a basic non-negative least squares calculation [41-43]. However, these values are default values, and in many cases, the variables are changed to be matched with the resultant Timur-Coates permeability with regard to the measured brine permeability.

Results and Discussion

In Table 1, the characteristics information of the core plug sample is provided. It comprises plug dimension, grain density, porosity, gas permeability, Klinkenberg permeability, and water permeability measured at ambient conditions. The grain density is consistent around 2.87 g/cm^3, indicating a carbonate rock sample. The permeability has been measured with gas and water, and the ratio of K_w/K_L indicates that the sample is relatively fully saturated with water.

NMR T_2 distribution has been measured on the same sample at room temperature with 5 wt.% NaCl brine and an echo spacing of 200 µs (microseconds).

This echo spacing is sufficiently short of capturing most of the short relaxation components from hydrogen atoms that occupy small pores and avoiding the unwanted influence of internal magnetic fields in the sample upon the signal. The raw echoes are converted to determine the T_2 distribution at dry, saturated and desaturated sample sate. The NMR analysis information is presented in Table 2.

The quality of NMR data has been assessed using the calculated ratio of signal to noise (S/N). The number of scans is adjusted for each measurement to aim for good signal quality. In this study, the quality of the NMR data is acceptable, and the ratio of signal to noise is higher than 200. This value is much higher than the signal quality achieved for log data.

The basic properties are determined from NMR analysis and core measurement. The results, however, are discussed as follows.

Pore Size Distribution

High-pressure mercury injection is performed on the carbonate rock sample from Asmari Formation. The cumulative mercury intrusion curve is shown in Figure 3 along with the Pc. The pore size distribution was determined from the mercury capillary pressure curve, and the result is presented in Figure 1. The MICP saturation curve shows that a low entry pressure of 15 psi is required to access the largest pores, and the flat capillary pressure hyperbola suggests good flow potential. The sample is interpreted to represent high reservoir quality.

Table 1 Characteristics information of the core sample from the core measurement

Sample ID	Length	Diameter	Vb	Vp	Vg	Porosity	Grain Density	Kg	Kl	Kw	Kw/Kl
	(cm)	(cm)	(cc)	(cc)	(cc)	(fraction)	(g/cm^3)	(mD)	(mD)	(mD)	
A	5.62	3.78	63.07	13.50	49.57	0.214	2.868	22.0	19.2	18.4	0.96

Table 2 NMR experiment information

Sample State	P90	P180	Gain	Echoes	N Scans	Mean T_2	S/N
	µs	µs	%			ms	
Dry	35.5	71.00	100	8000	6600	6.63	39
Saturated	35.5	71.00	100	32000	112	205.12	251
Desaturated	35.5	71.00	100	32000	80	321.43	233

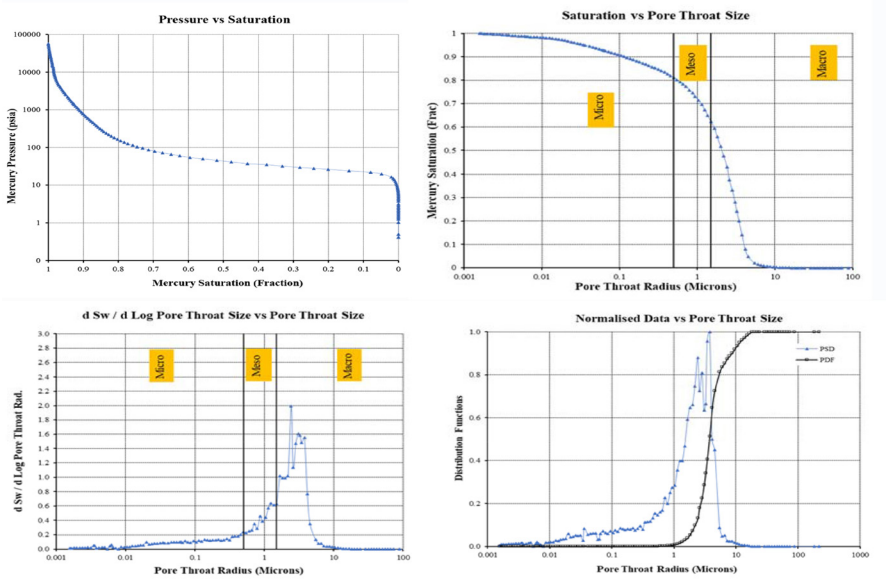

Fig 3. Mercury saturation and pore size distribution determined from MICP test.

The cumulative T_2 distribution for the completely saturated sample is shown in Figure 4. The T_2 distribution has had a negligible contribution to bulk fluid relation. Thus the result is equal to the distribution of surface relaxation time. Therefore, the pore size distribution is calculated by scaling factor (c) value of 0.015 micron/cm in Equation 9. As shown in Figure 5, the result is compared with the pore size distribution calculated from MICP data. The result shows that there is reliable consistency between two pore size distributions that had similar breadth. The mean dominant pore throat size determined from NMR and MICP is 5.5 microns.

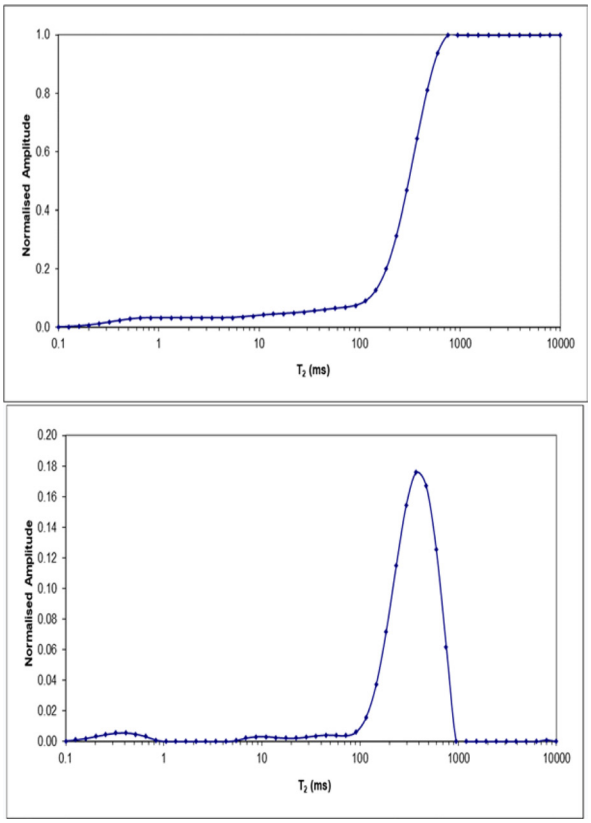

Fig. 4 T_2 distribution and cumulative T_2 distribution.

The thin section prepared from the sample cut-off is shown in Figure 6. A microcrystalline to fine-crystalline dolomitized mudstone. Open and anhydrite cemented hairline fractures are present in addition to microcrystallites. The thin section is characterized by a 1cm-diameter patch of microcrystalline dolomitized wackestone, which probably represents a burrow-infill with abundant benthic foraminifera and anhydrite-cemented biomoulds. The bioturbated mudstone precursor texture suggests deposition in a very low-energy, probably restricted environment.

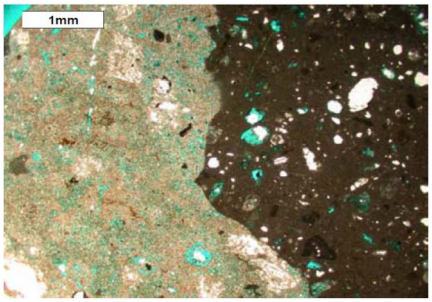

Fig. 6 Thin section from the core sample; Depth=1991.85 MD; MICP Porosity (%): 14.77; MICP Permeability (mD): 20.24.

However, the difference between the MICP and NMR-derived pore size curves is that the pores are assumed to be cylinders in NMR analysis, and the whole pore system has a uniform surface relaxivity. The NMR method processes the simple pore system with ideal pores. In contrast, the natural pore system shows complexity and variation in pore sizes. In a real porous medium, the pore has a different surface area to volume ratio than an ideal pore model with cylindrical shapes. The shape of pores will result in a different pore size distribution from the NMR technique rather than the pore size from the MICP method.

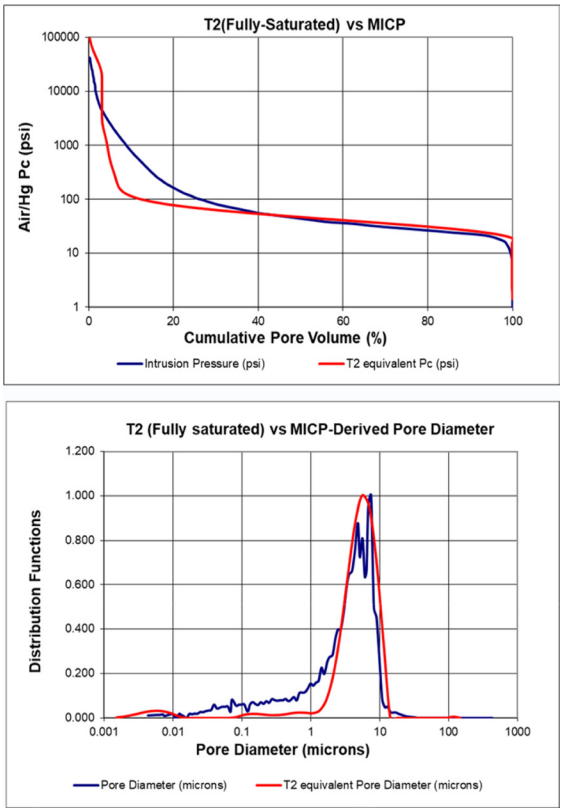

Fig. 5 Distribution of pore size and capillary pressure from MICP and NMR experiments.

Anhydrite occludes intercrystalline, mouldic/vuggy and fracture pore-space. However, the information from thin-section observations indicates good porosity hosted in intercrystalline micropores and locally connected mouldic/vuggy macropores. This is consistent with the MICP pore throat distribution with peaks at 5.5 μm that are associated with a mixed mesopore and macropore system.

Porosity

Porosity has been determined from core measurement and NMR T_2 distribution analysis. In Table 3, the porosity determined from two different methods is presented. A comparison of helium and NMR porosities shows that the NMR porosity is on average 0.72 porosity units lower than the helium porosity. This is due to the fact in the NMR method, the sample is completely saturated with the fluid, and the porosity is calculated using the brine saturated T_2 data. In contrast, the porosity of helium is determined by pore volumes filled with helium. Therefore, there might be a difference between the two measured porosities. Generally, this difference would be larger for a sample containing isolated pores, clays and bitumen or asphaltenes.

Table 3 Porosity and permeability are determined from core measurement and NMR.

Sample ID	He Porosity	NMR Porosity	Kg	KL	Mean T_2	SDR perm, mD		TC perm, mD	
	(%)	(%)	(mD)	(mD)	(ms)	(Standard)	(Optimized)	(Standard)	(Optimized)
A	21.4	20.68	22	19.2	205.12	770	17.7	0.82	18.0

Permeability

Permeability has been measured from core measurement and NMR T_2 distribution analysis. The standard Kenyon (SDR) and Timur-Coates (TC) equations are employed on the brine-saturated T_2 distributions. In Table 3, permeability results from the core measurement and NMR methods are given. The standard permeability predicting equations result in higher values compared to the core permeability. Therefore, the SDR and TC permeability models are manually optimized against core permeability by adjusting the pre-multiplier C and the exponents a and b. In Table 4, the parameters used for standard and optimized permeability models determined by SDR and Timur-Coates methods are presented. The optimized parameters are obtained with a try and error within a series of permeabilities.

Table 4 Parameters used to model permeability by SDR and TC.

Parameters	SDR perm, mD		TC perm, mD	
	standard	optimized	standard	optimized
A	2	1.6	2	2
B	4	3	4	4
C	0.001	0.0004	0.001	0.022
FFI	--	--	0.87	0.87
BVI	--	--	0.13	0.13

The procedure is that first, the permeability by the standard model is determined, and then a series of variable parameters are applied, and the consequent permeabilities are calculated. The square of the difference between the model permeability and measured permeability should be minimized. However, the parameters are optimized accordingly. The NMR measurements are done on 100% saturated and desaturated plug samples to determine the movable fluid (FFI) index and immobile fluid (BVI) for the Timur-Coates permeability model. Normalized T_2 distributions from saturated and desaturated (Swi) core plugs are first plotted in Figure 7, and the intercept identifies T_2 cut-off for FFI and BVI. In this study, Swi has been determined to be 0.14, and T_2 cut-off is 135 milliseconds (ms). Therefore, the FFI and BVI have been determined to be 0.87 and 0.13, respectively, as shown in Figure 8.

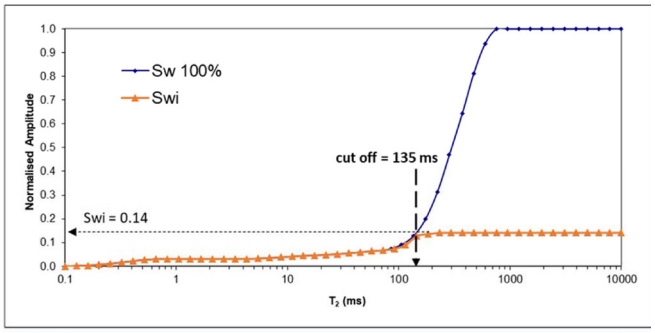

Fig. 7 Normalized T_2 distribution for saturated and desaturated plug.

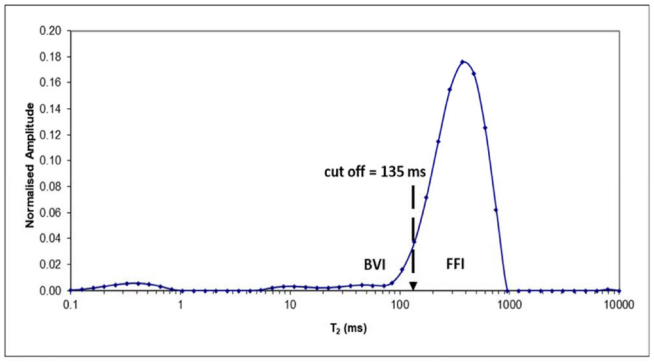

Fig. 8 FFI and BVI determination (T_2 cut off = 135 ms).

The result shows that the standard models systematically overpredict laboratory permeability. The optimized version of the SDR and TC equations substantially improves permeability predictions for the sample, as shown in Table 5. The ratio of model permeability to the measured permeability is 40 for the standard SDR method, while the ratio has improved to 0.921 with optimized model permeability. The ratio is 0.043 for the standard TC equation while it is 0.938 with the optimized parameters.

Table 5 The ratio of model permeability to measured permeability by SDR and TC methods.

K_{model} / K_{core}	SDR perm, mD		TC perm, mD	
	standard	optimized	standard	optimized
	40	0.921	0.043	0.938

Figure 9 shows the permeability results from the SDR and TC models, and the results between the standard and optimized equations are compared. The result shows that the standard procedure gives biased values while the optimized model will adjust results reasonably matched with core permeability values.

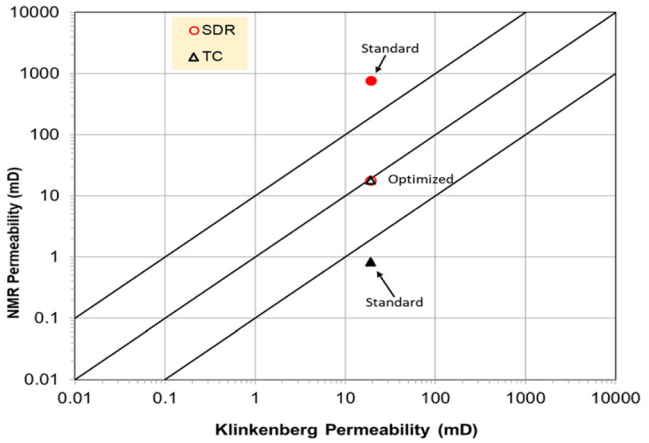

Fig. 9 NMR vs Kl permeability for standard and optimized SDR and TC models.

Conclusions

In this paper, data from core measurement and NMR experiments are investigated for Asmari carbonate Formation. The sample is a 1.5-inch diameter core plug, and measurements of air permeability, grain density and helium porosity are conducted at the clean state. On the other hand, the petrophysical parameters of the plug were investigated by NMR analysis in the laboratory. The porosity values of the NMR technique (20.68 %) and the He porosity test (21.4%) presented a reliable correlation. An excellent match between pore size distributions resulting from the NMR model and MICP experiment is distinguished. Permeability values are also predicted using two standard NMR models namely standard SDR and Timur-Coates (TC). The values have been optimized and compared with CCAL permeability data. The study results demonstrate that NMR could be considered as an acceptable substitutional method in the petrophysical study of Asmari carbonate reservoir as major petrophysical parameter results, porosity permeability values, show reliable consistency (average core and NMR porosity are 21.4 % and 20.68%; average core and NMR permeability are 17.85 (mD) and 19.85 (mD) respectively). An integrated core, NMR and petrophysical study could reduce the uncertainties in upcoming exploration and development projects in Asmari Formation.

Nomenclatures

A: Cross section area (cm^2)
BVI: Bulk volume irreducible
CPMG: Carr-Purcell-Meiboom-Gill
D: Diameter (cm)
FFI: Free fluid index
FS: Shape factor which is related to the pore throat
Kg: Gas permeability
KI: Klinkenberg permeability
Kr: Relative permeability
Kw: Water permeability
L: Length (cm)
M: Initial magnetization at time zero
MICP: Mercury Injection Capillary Pressure
NMR: Nuclear Magnetic Resonance
PA: Atmospheric Pressure
P1: Inlet pressure
P2: Outlet Pressure
Pc: Capillary Pressure
Q: Gas flow rate (cc/s)
RCAL: Routine Core Analysis
S: Pore surface area (cm^2)
SCAL: Special core analysis
SDR: Schlumberger-Doll-Research
SW: Water saturation
T2: Nuclear magnetic resonance transverse relaxation time distribution
TC: Timur-Coates techniques
Vb: Bulk volume
Vg: Grain volume
Vo: Fluid volume
Vp: Pore Volume
Wt: Dry sample volume
ρ2: Surface relaxation constant
δ: Surface tension of mercury
θ: Contact angle, mercury/solid

References

1. Kerans C, Lucia F J, Senger R K (1994) Integrated characterization of carbonate ramp reservoirs using Permian San Andres Formation outcrop analogs, AAPG bulletin, 181-216.
2. Yarmohammadi S, Kadkhodaie A, Hosseinzadeh S (2020) An integrated approach for heterogeneity analysis of carbonate reservoirs by using image log based porosity distributions, NMR T2 curves, velocity deviation log and petrographic studies: A case study from the South Pars gas field, Persian Gulf Basin, Journal of Petroleum Science and Engineering, 192:107283.
3. Tiab D, Donaldson E (2015) Petrophysics, 4th Edition, Gulf Professional Publishing.
4. Fitch P J R, Lovell M A, Davies S J, Pritchard T, Harvey P K (2015) An integrated and quantitative approach to petrophysical heterogeneity, Marine and Petroleum Geology, 63: 82–96.
5. Kenyon W E (1997) Petrophysical principles of applications of NMR logging, The log analyst, 38: 02.
6. Darmawan C, Rosid M, Rulliyansyah R (2018) Characterization of carbonate reservoir by using nuclear magnetic resonance (NMR) logging analysis at hydrocarbon field c south sumatera, AIP Conference Proceedings 1: 020261-1–020261-6.
7. Kadkhodaie A, Yarmohammadi S (2019) Carbonate microfacies study by using images processing algorithms, k-mean clustering and nearest neighbor segmented classifying: an example from the salman oil and gas field, Persian Gulf, Iran, Geopersia, 10, 2: 277-287.
8. Knackstedt M, Jaime P, Butcher A R, Botha P W, Middleton J, Sok R (2010) Integrating reservoir characterization: 3D dynamic, petrophysical and geological description of reservoir facies, In SPE Asia Pacific Oil and Gas Conference and Exhibition, OnePetro.
9. Ahmed T (2018) Reservoir engineering handbook, 1st edition, Gulf professional publishing.
10. Rios E, Figueiredo I, Muhammad A, Azeredo R, Moss A, Pritchard T, Glassborow B (2014) NMR permeability estimators under different relaxation time selections: a laboratory study of cretaceous diagenetic chalks, SPWLA 55th Annual Logging Symposium, OnePetro.
11. Akkurt R, Cherry R (2001) NMR Logging Applications, SPWLA 42nd Annual Logging Symposium Houston Texas, 113 pp.
12. Westphal H, Surholt I, Kiesl C, Thern H, Krupse T (2005) NMR measurements in carbonate rocks: problems and an approach to a solution, Pure applied geophysics, 162, 3: 549–570.
13. Benavides F, Leiderman R, Souza A, Carneiro G, de Vasconcellos Azeredo R G (2019) Pore size distribution from NMR and image based methods: A comparative study, Journal of Petroleum Science and Engineering, 184, 106321.
14. Rothwell WP, Vinegar H J (1985) Petrophysical

applications of NMR imaging, Applied optics, 24 23: 3969-3972.
15. Marschall D, Gardner JS, Mardon D, Coates G R (1995) Method for correlating NMR relaxometry and mercury injection data, Society of Core Analysis Conference, 9511: 40.
16. Altunbay M, Martain R, Robinson M (2001) Capillary pressure data from nmr logs and its implications on field economics, Society of Petroleum Engineers, 71703.
17. Mao Z Q, Yu-Dan H E, Ren X J (2005) An Improved Method of Using NMR T2 Distribution to Evaluate Pore Size Distribution, Chinese Journal of Geophysics, 48, 2: 412–418.
18. Daigle H, Thomas B, Rowe H, Nieto M (2014) Nuclear magnetic resonance characterization of shallow marine sediments from the Nankai Trough, integrated ocean drilling program expedition 333, Journal of Geophysics Research Solid Earth,119: 2631–2650.
19. Kaufman L, Crooks L E (1994) NMR Imaging, Journal of Appled Physics, 57, 1: 2989-2995.
20. Amabeoku M, Funk J, Al-Dossary S, Al-Ali H (2001) calibration of permeability derived from nmr logs in carbonate reservoirs, Society of Petroleum Engineers: 68085.
21. Motiei H (1993) Stratigraphy of Zagros, Geological Survey of Iran, 1-536.
22. Alizadeh B, Maroufi K, Fajrak M (2018) Hydrocarbon reserves of Gachsaran oilfield, SW Iran: Geochemical characteristics and origin, Marine and Petroleum Geology, 92: 308-318.
23. Dill M A, Seyrafian A, Vaziri-Moghaddam H (2010) The Asmari Formation, north of the Gachsaran (Dill anticline), southwest Iran: facies analysis, depositional environments and sequence stratigraphy, Carbonates and Evaporites 25, 2: 145-160.
24. Vaziri-Moghaddam H, Kimiagari M, Taheri A (2006) Depositional environment and sequence stratigraphy of the Oligo-Miocene Asmari Formation in SW Iran, Facies, 52,1: 41-51.
25. Sepehr M, Cosgrove J W (2004) Structural framework of the Zagros fold–thrust belt, Iran. Marine and Petroleum geology, 21, 7: 829-843.
26. Dickson J (1965) A Modified Staining Technique for Carbonates in Thin Section, Nature, 205, 4971: 205-587.
27. Fang T, Zhang L, Liu N, Zhang L, Wang W, Yu L, Li C, Lei Y (2018) Quantitative characterization of pore structure of the Carboniferous–Permian tight sandstone gas reservoirs in eastern Linqing depression by using NMR technique, Petroleum Research, 3: 110–123.
28. Kleinberg R, Farooqui S, Horsfield M (1993) T1/T2 ratio and frequency dependence of NMR relaxation in porous sedimentary rocks, Journal of Colloid and Interface Science, 158, 1:195-198.
29. Gong Y, Liu S, Zhao M, Xie H, Liu K (1999) Characterization of micro pore throat radius distribution in tight oil reservoirs by NMR and high pressure mercury injection, Petroleum Geolology Exp, 38: 389–394.
30. Hamada G M, Al-behed M N J, Al-awad M N J (1999) NMR logs find reserves by-passed by conventional analysis, Oil and Gas Journal, 97: 75–80.
31. Howardt J, Kenyon W (1992) Determination of pore size distribution in sedimentary rocks by proton nuclear magnetic resonance, Marine and Petroleum Geology, 9, 2: 139-145.
32. Keeler J (2010) Understanding_NMR_Spectroscopy, 2nd edition University of Cambridge, Department of Chemistry.
33. Lyu C, Ning Z, Wang Q, Chen M (2018) Application of NMR T2 to pore size istribution and movable fluid distribution in tight sandstones, American Chemical Society- Energy and Fuels, 32, 2:1395-1405.
34. Xu H, Fan Y, Hu F, Li C, Yu J, Liu Z, Wang F (2019) Characterization of pore throat size distribution in tight sandstones with nuclear magnetic resonance and high-pressure mercury intrusion, Energies, 12: 1528.
35. Xiao L, Mao Z, Zou C, Li J, JinY (2012) Calculation of porosity from nuclear magnetic resonance and conventional logs in gas-bearing reservoirs, Acta Geophysica, 60:4, 1030-1042.
36. Kharraa H, Al-Amri M, Mahmoud M, Okasha T (2013) Assessment of uncertainty in porosity measurements using NMR and conventional logging tools in carbonates reservoirs, Society of Petroleum Engineers, 168110.
37. Kenyon W E, Day P I, Straley C, Willemesen J F (1995) A Three-part Study of NMR longitudinal relaxation properties of water-saturated sandstones. SPE formation evaluation, 3, 03: 622-636.
38. Kenyon B, Kleinberg R, Straley C, Etc (1986) Nuclear Magnetic Resonance Imaging Technology for the 21st Century, Oilfield Review, 15.
39. Timur A (1968) An investigation of permeability, porosity and residual water saturation relationships, SPWLA Annual Logging Symposium SPWLA.
40. Coates G R, Denoo S (1988) The Producibility Answer Product, Schlumberger Technical Review, 29, 2: 55.
41. Wei D F, Liu X P, Hu X X, Xu R, Zhu L L (2015) Estimation of permeability from NMR logs based on formation classification method in tight gas sands, Acta Geophysica, 63, 5: 1316-1338.
42. Trevizan W, Netto P, Coutinho B, Machado V F, Rios E H, Chen S, Romero, P (2014) Method for predicting permeability of complex carbonate reservoirs using NMR logging measurements, Petrophysics-The SPWLA Journal of Formation Evaluation and Reservoir Description, 55, 03: 240-252.
43. Yujiao H, Cancan Z, Yiren F, Chaoliu L, Chao Y, Yunhai C (2018) A new permeability calculation method using nuclear magnetic resonance logging based on pore sizes: A case study of bioclastic limestone reservoirs in the A oilfield of the Mid-East, Petroleum Exploration and Development, 45,1:183-192.